IL NUOVO CIMENTO **43 C** (2020) 119
DOI 10.1393/ncc/i2020-20119-y

COMMUNICATIONS: SIF Congress 2019

Supernova neutrino detection in XENONnT neutron and muon Vetoes

F. POMPA(1)(2)

(1) *INFN, Sezione di Bologna - Bologna, Italy*
(2) *Dipartimento di Fisica, Università di Bologna - Bologna, Italy*

received 27 January 2020

Summary. — The current phase of the XENON Dark Matter Project, named XENONnT, will be operative in 2020 in the underground Laboratori Nazionali del Gran Sasso (LNGS). It is a multi-ton detector for direct search of Dark Matter, consisting of a double phase liquid-gas xenon Time Projection Chamber (TPC) which contains 5.9 tons of liquid xenon target mass, inserted in a cryostat surrounded by a tank containing 700 tons of water doped with Gd sulphate. Its aim, as that of its precursor XENON1T, is to detect elastic scattering of Weakly Interacting Massive Particles (WIMPs) off xenon nuclei. The presence of two Veto sub-systems, the muon Veto instrumented with 84 photomultiplier tubes (PMTs) and the neutron Veto with other 120 PMTs, allows to reduce the background for WIMPs search through muon and neutron tagging, while the presence of Gd sulphate increases the neutron capture cross section. Thanks to the large xenon target used and the presence of the two Vetoes, XENONnT will be able also to detect all flavours of Supernova neutrinos. Here the results from Monte Carlo simulations of XENONnT detection efficiency are presented for Supernova neutrinos through their inverse beta decay interactions in water of the two Veto sub-systems.

1. – Introduction

There are justified reasons to believe that new phenomena, new particles and new principles that would lead us to a deeper level of understanding of nature, are waiting for us beyond the description given today by the Standard Model of particle physics. Indeed, some considerations show that the Standard Model is incomplete and can be seen as a *low-energy limit* of a more fundamental theory, which should reveal itself at higher energies. A lot of astrophysical and cosmological observations support the hypothesis that a considerable amount of the energy content of the Universe is made of something we do not know and that is called Dark Matter. Candidate particles for Dark Matter arise from theories beyond the Standard Model with the properties of stable or very long lives, no electric and colour charge and non-relativistic nature. Due to such features,

these candidates are identified with the name of Weakly Interacting Massive Particles (WIMPs) [1]. The number of experiments to directly detect WIMPs has grown in the last years. Currently, the XENON Project at LNGS has a leading role in this field, exploiting the technique of the double-phase TPC based on xenon [2]. Another evidence of something beyond the known physics is the definitive discovery of a non-zero neutrino mass. With its unknown mass and uncertain Dirac or Majorana nature, neutrino is waiting to be placed into a new model, different from the Standard Model which cannot describe it in the correct way. Dark Matter detectors have now achieved tonne-scale targets, giving them sensitivity to neutrinos of all flavours coming from Supernovae. During a Supernova explosion, most of the energy is released by neutrinos and antineutrinos of all flavours, with mean energies of $\mathcal{O}(10)$ MeV. In this scenario, neutrinos are an important tool to study the dynamics of the explosion. With XENONnT, Supernova neutrinos can be detected through two different interaction channels: via coherent elastic scattering of neutrinos with xenon nuclei (CEνNS) [3] in the TPC and through inverse beta decay (IBD) processes in water. In the following, the possibility to detect Supernova neutrinos with the XENONnT neutron and muon Vetoes is presented, focusing on the IBD channel.

2. – XENONnT

The current phase of the XENON Dark Matter Project is XENONnT, hosted at LNGS in the same support structure of its precursor XENON1T [4], which was built with the capability to rapidly increase its sensitivity target. It is a double-phase TPC detector containing about 8 tons of xenon. This TPC has an height of about 1.6 m, a diameter of 1.3 m and its active volume contains 5.9 tons of xenon, observed by two arrays of PMTs, the top array with 253 PMTs and the bottom one with 241 PMTs. This TPC is inserted into a cryostat, containing the remaining tons of xenon and placed into a 10.2 m high tank with a diameter of 9.6 m, filled with Gd-doped water. The cryostat is surrounded by two sub-detectors: a muon Veto Čerenkov detector, instrumented with 84 PMTs and a new octagonal structure, the neutron Veto, instrumented with 120 PMTs. The presence of these Veto sub-systems allows to reduce the background rate in the TPC. Furthermore, the presence of gadolinium in water, at 0.2% mass concentration, increases the neutron capture cross section, allowing to further reduce the nuclear recoil background in the TPC.

3. – Supernova neutrino fluxes and oscillations

Core collapse Supernovae are among the most energetic events occurring in our Universe, originated from the death of stars with masses $M > 8M_{\odot}$. Most of the energy emitted by the explosion is released by neutrinos and antineutrinos of all flavours, with mean energies of about $\mathcal{O}(10)$ MeV. The differential flux for each neutrino flavour ν_β at a time t_{pb} after the Supernova core bounce at a distance d is parametrized by [3]

$$\Phi_{\nu_\beta}(E, t_{\mathrm{pb}}) = \frac{L_{\nu_\beta}(t_{\mathrm{pb}})}{4\pi d^2} \frac{\varphi_{\nu_\beta}(E, t_{\mathrm{pb}})}{\langle E_{\nu_\beta}(t_{\mathrm{pb}})\rangle}, \tag{1}$$

where $L_{\nu_\beta}(t_{\rm pb})$ is the ν_β luminosity, $\langle E_{\nu_\beta}(t_{\rm pb})\rangle$ its mean energy and $\varphi_{\nu_\beta}(E, t_{\rm pb})$ is the neutrino energy distribution, defined as

$$\varphi_{\nu_\beta}(E, t_{\rm pb}) = \xi_\beta(t_{\rm pb}) \left(\frac{E}{\langle E_{\nu_\beta}(t_{\rm pb})\rangle} \right)^{\alpha_\beta(t_{\rm pb})} \exp\left\{ \frac{-[\alpha_\beta(t_{\rm pb}) + 1]E}{\langle E_{\nu_\beta}(t_{\rm pb})\rangle} \right\}. \tag{2}$$

The parameter $\alpha_\beta(t_{\rm pb})$ satisfies the relation

$$\alpha_\beta(t_{\rm pb}) = \frac{2\langle E_{\nu_\beta}(t_{\rm pb})\rangle^2 - \langle E^2_{\nu_\beta}(t_{\rm pb})\rangle}{\langle E^2_{\nu_\beta}(t_{\rm pb})\rangle - \langle E_{\nu_\beta}(t_{\rm pb})\rangle^2}, \tag{3}$$

while $\xi_\beta(t_{\rm pb})$ is a normalization factor defined such that

$$\int \varphi_{\nu_\beta}(E, t_{\rm pb}) {\rm d}E = 1. \tag{4}$$

In the following, the attention is focused on a Supernova progenitor of mass $M = 27 M_\odot$ in the *Lattimer* and *Swesty* equation of state with a nuclear incompressibility modulus of $k = 220\,{\rm MeV}$ (LS220 EoS) [5].

The phenomenon of neutrino flavour oscillations, first predicted by Pontecorvo [6] and connected with the non-zero neutrino mass, modifies the neutrino fluxes. In the standard three-flavours scenario, neutrino mixing and oscillations can be formally treated in the same manner as for the quark sector [7]: the three known flavour eigenstates ν_l ($l = e, \mu, \tau$) are mixed with the three mass eigenstates n_k ($k = 1, 2, 3$) through the unitary Pontecorvo-Maki-Nakagawa-Sakata mixing matrix U,

$$\nu_l = \sum_{k=1}^{3} U_{lk} n_k. \tag{5}$$

Here extra phases, possible if neutrinos are Majorana particles, are neglected, since these are not relevant in oscillations. The current neutrino phenomenology implies that the three-neutrino mass spectrum m_k ($k = 1, 2, 3$) is composed of a doublet of relatively close states and of a third lone neutrino state, which may be either heavier than the doublet (normal ordering, NO) or lighter (inverted ordering, IO) [8]. Typically, the lightest neutrino in the doublet is n_1 and the heaviest one is n_2: the corresponding mass squared difference $\Delta m^2_{\rm sol}$, called solar mass squared difference, is defined, by convention, as

$$\Delta m^2_{\rm sol} = m_2^2 - m_1^2 > 0. \tag{6}$$

The lone state is then labelled as n_3. The second independent mass squared difference $\Delta m^2_{\rm atm}$, called atmospheric mass squared difference, is defined as

$$\Delta m^2_{\rm atm} = \left| m_3^2 - \frac{m_1^2 + m_2^2}{2} \right|, \tag{7}$$

and its physical sign distinguishes the ordering of neutrino mass spectrum: in the normal ordering case $\Delta m^2_{\rm atm} > 0$ with $m_1 < m_2 < m_3$ while, in the inverted one, $\Delta m^2_{\rm atm} < 0$

with $m_3 < m_1 < m_2$. The existing data do not allow to determine its sign. Numerically, it results that

$$|\Delta m^2_{\rm atm}| \gg \Delta m^2_{\rm sol}. \tag{8}$$

The measurement of a large value of the mixing angle $\theta_{13} \simeq 8.13^\circ$ has significantly reduced the ambiguity in characterizing the Supernova neutrino oscillations. Streaming through the outer layers of the stellar envelope, as the Supernova matter potential declines, neutrinos and antineutrinos would feel ordinary matter effects. In their path from the high-density region where they are generated to the lower-density one where they escape the star, neutrinos and antineutrinos cross two resonance layers, called Mikheyev-Smirnov-Wolfenstein resonance layers [9]. The oscillation scheme of Supernova neutrinos for normal ordering is [10]

$$\Phi_{\nu_e} = P_H U^2_{e2} \Phi^0_{\nu_e} + (1 - P_H U^2_{e2}) \Phi^0_{\nu_x}, \tag{9a}$$

$$\Phi_{\bar\nu_e} = U^2_{e1} \Phi^0_{\bar\nu_e} + U^2_{e2} \Phi^0_{\bar\nu_x}, \tag{9b}$$

while the one for inverted ordering is

$$\Phi_{\nu_e} = U^2_{e2} \Phi^0_{\nu_e} + U^2_{e1} \Phi^0_{\nu_x}, \tag{10a}$$

$$\Phi_{\bar\nu_e} = P_H U^2_{e1} \Phi^0_{\bar\nu_e} + (1 - P_H U^2_{e1}) \Phi^0_{\bar\nu_x}, \tag{10b}$$

where P_H is the probability to jump onto an adjacent mass eigenstate crossing the high-density resonance layer, Φ^0 is the non-oscillated flux and, from the neutrino mixing matrix U,

$$U^2_{\rm e1} = \cos^2\theta_{13} \cos^2\theta_{12} \simeq \cos^2\theta_{12}, \tag{11a}$$

$$U^2_{\rm e2} = \cos^2\theta_{13} \sin^2\theta_{12} \simeq \sin^2\theta_{12}. \tag{11b}$$

Here ν_x indicates ν_μ and ν_τ, while $\bar\nu_x$ their respective antineutrinos. In the study of Supernova neutrinos these are indistinguishable because the differences in their interactions are rather small and, correspondingly, their emitted spectra are very similar. For typical Supernova simulations, the matter density profile declines so slowly that the neutrino propagation is adiabatic, so the flip probability is null: $P_H = 0$. The oscillation schemes of eqs. (9) and (10) become

$$\Phi_{\nu_e} = \Phi^0_{\nu_x}, \tag{12a}$$

$$\Phi_{\bar\nu_e} = \cos^2\theta_{12} \Phi^0_{\bar\nu_e} + \sin^2\theta_{12} \Phi^0_{\bar\nu_x}, \tag{12b}$$

for the normal ordering and

$$\Phi_{\nu_e} = \sin^2\theta_{12} \Phi^0_{\nu_e} + \cos^2\theta_{12} \Phi^0_{\nu_x}, \tag{13a}$$

$$\Phi_{\bar\nu_e} = \Phi^0_{\bar\nu_x}, \tag{13b}$$

for the inverted one. Replacing the numerical values of $\sin^2\theta_{12}$ and $\cos^2\theta_{12}$, the neutrino fluxes of figs. 1 and 2 are obtained, respectively, for the normal ordering case and the inverted one: here the comparison is shown between the non-oscillated fluxes (grey lines) and the neutrino flavour oscillations effects (black lines).

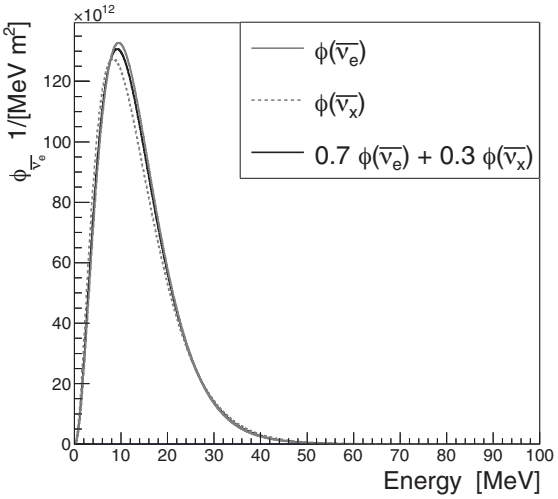

Fig. 1. – Comparison between fluxes of $\bar{\nu}_e$ (solid grey line), $\bar{\nu}_x$ (dotted grey line) and $\bar{\nu}_e$ oscillated in NO (solid black line) for the $27M_\odot$ progenitor star in LS220 EoS.

4. – Inverse beta decay process

Here the focus is on the interactions of Supernova electron antineutrinos in water through inverse beta decay processes:

$$\bar{\nu}_e + p \longrightarrow n + e^+. \tag{14}$$

Emitted positrons have an energy spectrum given by

$$E_{e^+} = E_{\bar{\nu}_e} - 1.806\,\mathrm{MeV}, \tag{15}$$

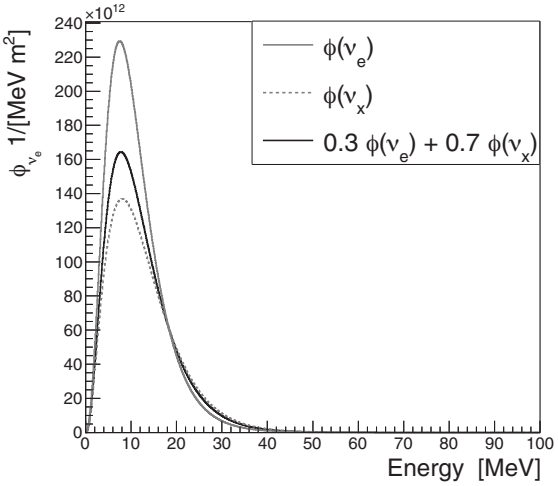

Fig. 2. – Comparison between fluxes of ν_e (solid grey line), ν_x (dotted grey line) and ν_e oscillated in IO (solid black line) for the $27M_\odot$ progenitor star in LS220 EoS.

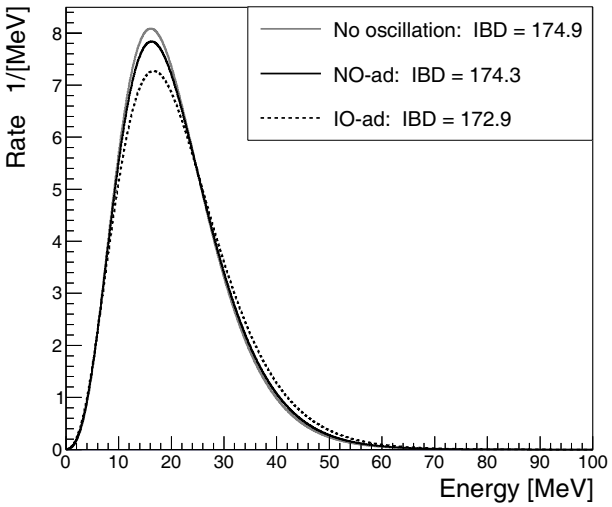

Fig. 3. – Comparison between spectra of positrons produced via IBD from interaction of non-oscillated $\bar{\nu}_e$ (grey line), oscillated $\bar{\nu}_e$ in NO (solid black line) and oscillated $\bar{\nu}_e$ in IO (dotted black line).

while neutrons have energies of few keV. Positrons and captured neutrons produce Čerenkov light in Gd-doped water that can be detected by the PMTs of muon Veto and neutron Veto. Considering a target mass of 700 tons of water, with the non-oscillated electron antineutrino spectum given by the solid grey line of fig. 1, the total number of expected IBD interactions is about 175. Neutrino oscillations do not modify significantly this number. Considering always the same target mass of water, fig. 3 illustrates the results obtained: in adiabatic conditions and in case of mass spectrum with normal ordering (solid black line), we expect about 174 IBD interactions while, in case of mass spectrum with inverted ordering (dotted black line), we expect about 173 IBD interactions. Because of the very slight variation between these numbers, the following study involves the non-oscillated scenario.

Both positrons and neutrons, products of IBD interactions, were generated through Monte Carlo simulations, performed using the XENONnT GEANT4 code. Below, the XENONnT detection efficiencies of both these signals are obtained.

5. – Detection efficiency of positrons and neutrons in water

Through Monte Carlo simulations, 10^5 positrons of energy given by eq. (15) and 10^5 neutrons of 1 keV energy, products of IBD interactions of non-oscillated electron antineutrinos, are generated uniformly in the whole water volume. To get an idea about the number of events generated in each Veto sub-system, it is possible to consider their respective volumes:

- muon Veto volume: $610\,\mathrm{m}^3$,
- neutron Veto volume: $53\,\mathrm{m}^3$.

As these values show, most of the events are generated outside the neutron Veto. Requiring a certain PMTs multiplicity, without any distinction between the two Vetoes, the

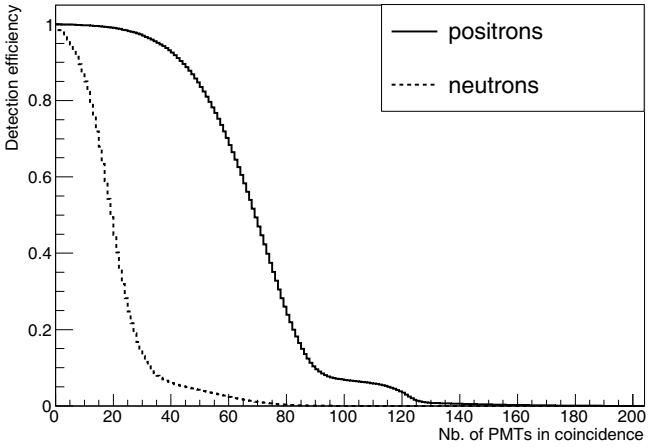

Fig. 4. – Comparison between total detection efficiency of positrons (solid black line) and neutrons (dotted black line), without any distinction between the two Vetoes.

efficiency plots of fig. 4 are obtained: the solid black line represents the positron detection efficiency as a function of the number of PMTs required in coincidence, while the black dotted one is the neutron detection efficiency. With the coincidence of 10 PMTs, the total detection efficiency of simulated positrons is $\epsilon_{e^+} = 0.99$ while the one of simulated neutrons is $\epsilon_n = 0.87$. Given these values, it is possible to compute the number of detected IBD interactions: generally, not all the expected events are effectively observed. Taking into account the neutrino oscillations, considering another Supernova progenitor of mass $M = 11.2M_\odot$ and another equation of state, the *Shen* one [5], the comparison between the expected number of IBD events and the detected one with 10 PMTs in coincidence is shown in table I. Thanks to the high values of detection efficiency, almost all IBD events are detected in each case. The total energy deposited by positrons and neutrons in water

TABLE I. – *Comparison between different numbers of expected IBD interactions and detected IBD interactions, requiring* 10 *PMTs in coincidence, coming from different Supernova progenitors in both the equations of state used and mass orderings. Thanks to the high values of detection efficiency, almost all IBD events are detected.*

Solar mass	EoS	Mass ordering	Expected IBD	Detected IBD
$27M_\odot$	LS220	NO	174.3	173.9
		IO	172.9	172.5
	Shen	NO	135.0	134.7
		IO	121.7	121.4
$11.2M_\odot$	LS220	NO	87.4	87.2
		IO	87.9	87.7
	Shen	NO	71.9	71.8
		IO	68.1	67.9

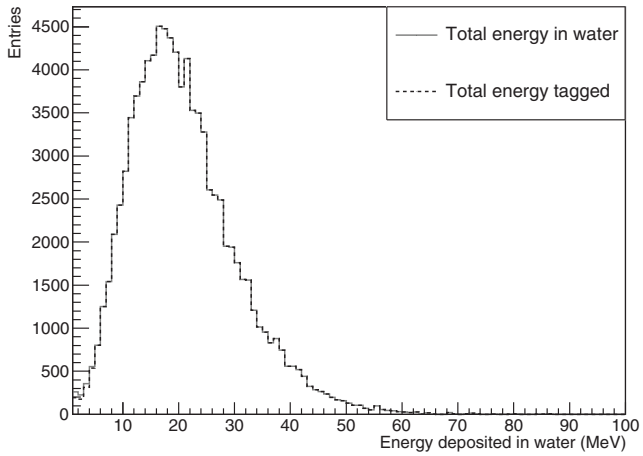

Fig. 5. – Comparison between total energy deposited by positrons in water (solid grey line) and total energy tagged with 10 PMTs in coincidence (black dotted line). For energies greater than 6 MeV all events are tagged.

is reported, respectively, in figs. 5 and 6: here, solid grey lines represent the total energy deposited in water by particles, while the black dotted ones illustrate the total energy tagged in both cases with 10 PMTs in coincidence. In the positron case, for energies greater than 6 MeV, all events are tagged, while for neutrons two peaks, corresponding to the capture of neutrons on protons (around 2 MeV) and on Gd nuclei (around 8 MeV), are evident.

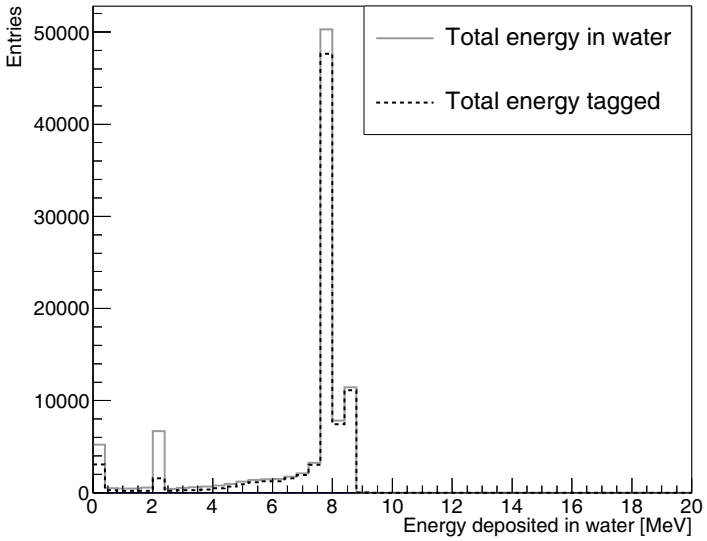

Fig. 6. – Comparison between total energy deposited by neutrons in water (solid grey line) and total energy tagged with 10 PMTs in coincidence (black dotted line). Two peaks, corresponding to the capture of neutrons on protons (around 2 MeV) and on Gd nuclei (around 8 MeV), are shown.

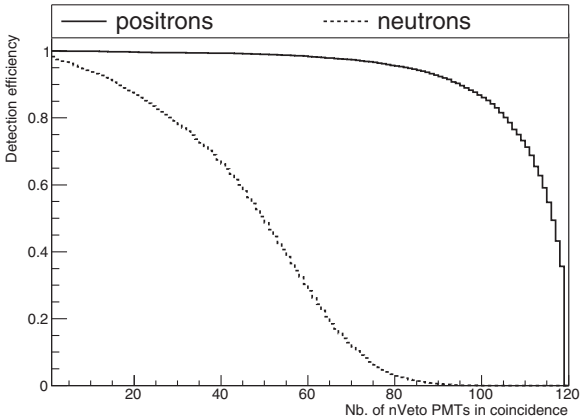

Fig. 7. – Detection efficiency of the neutron Veto for positrons (solid black line) and neutrons (black dotted line) generated inside the neutron Veto itself.

A separate analysis on neutron Veto and muon Veto, considering events generated only in their respective volumes, produced the results of figs. 7 and 8: solid black lines are referred to the positron detection efficiency while black dotted ones to the neutron detection efficiency. Always requiring 10 PMTs in coincidence, both the Veto sub-systems measured a positron detection efficiency of $\epsilon_{e^+} = 0.99$. In the neutron case, neutron Veto obtained a detection efficiency of $\epsilon_n = 0.94$ while the muon Veto measured an efficiency of $\epsilon_n = 0.85$. The difference in the values of positron and neutron detection efficiency is due to the fact that positrons, being charged particles, release all their energy in water through Čerenkov light, while neutrons must be captured before being detected.

The distribution of photoelectrons in neutron and muon Vetoes is showed, respectively, by figs. 9 and 10 in the positron case, and by figs. 11 and 12 in the neutron case. Black lines show the distribution of the total number of photoelectrons, grey dotted

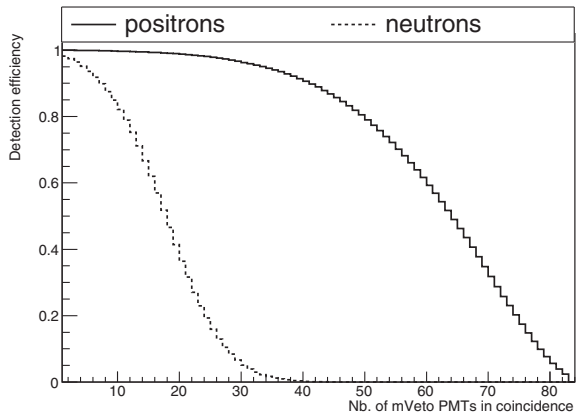

Fig. 8. – Detection efficiency of the muon Veto for positrons (solid black line) and neutrons (black dotted line) generated inside the muon Veto itself.

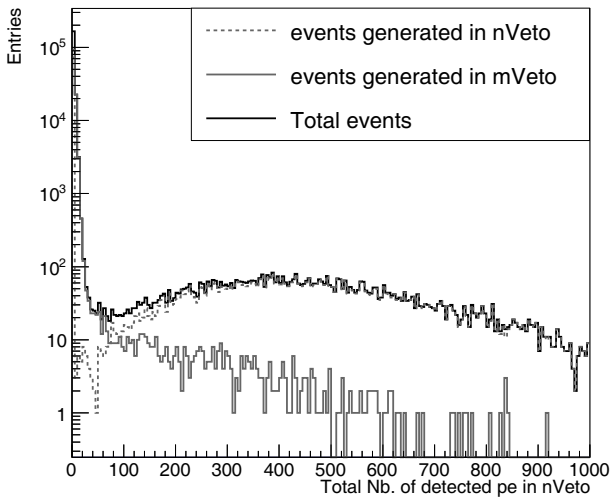

Fig. 9. – Distribution of the total number of photoelectrons produced following the interactions of positrons in the neutron Veto. The solid grey line illustrates the contribution of events generated inside the muon Veto, while the dotted grey line shows the one of events generated in the neutron Veto itself. The black line is the sum of the two contributions.

lines represent the contribution due to events generated in the considered Veto, while solid grey lines illustrate the contribution due to events generated in the other Veto. As expected, most of the detected light is produced by events generated in the Veto we are considering.

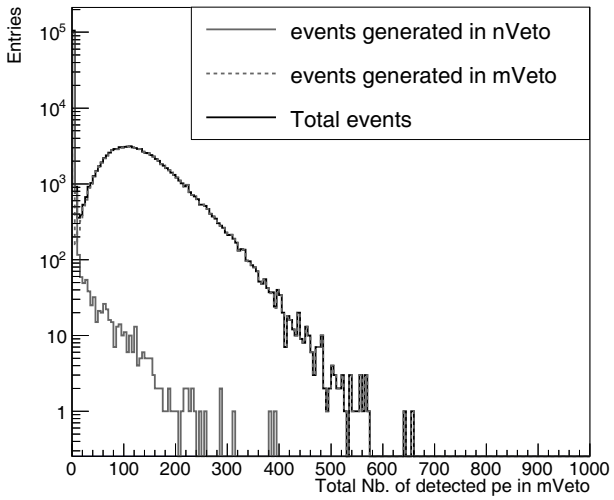

Fig. 10. – Distribution of the total number of photoelectrons produced following the interactions of positrons in the muon Veto. The solid grey line illustrates the contribution of events generated inside the neutron Veto, while the dotted grey line shows the one of events generated in the muon Veto itself. The black line is the sum of the two contributions.

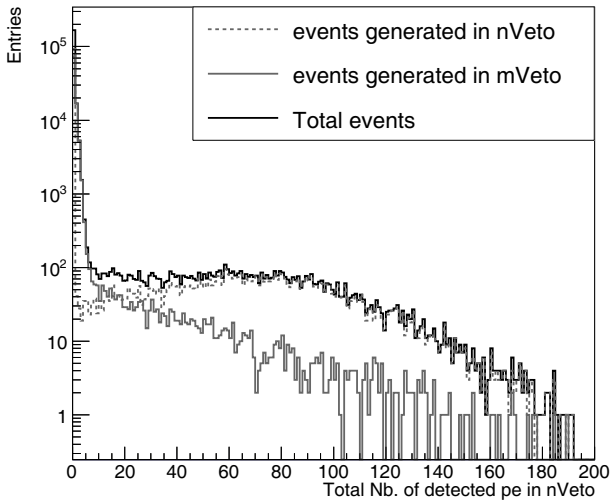

Fig. 11. – Distribution of the total number of photoelectrons produced following the interactions of neutrons in the neutron Veto. The solid grey line illustrates the contribution of events generated inside the muon Veto, while the dotted grey line shows the one of events generated in the neutron Veto itself. The black line is the sum of the two contributions.

These results demonstrate that a high detection efficiency can be obtained for both the products of IBD interactions of Supernova neutrinos. The combined detection of positrons and neutrons, inside the few seconds window typical of Supernova neutrino emission, allows XENONnT to be sensitive to this very rare and precious signal.

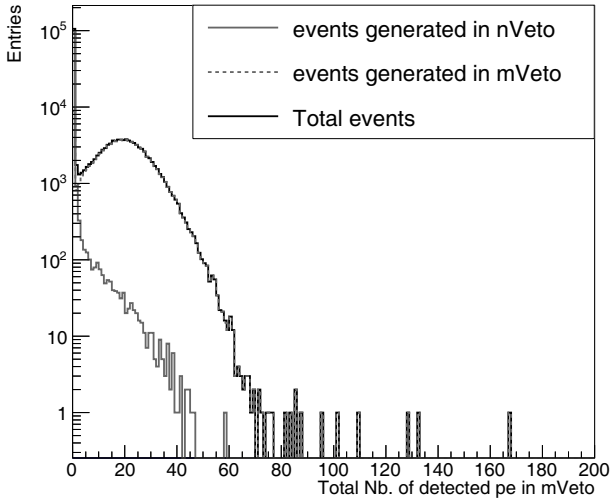

Fig. 12. – Distribution of the total number of photoelectrons produced following the interactions of neutrons in the muon Veto. The solid grey line illustrates the contribution of events generated into the neutron Veto, while the dotted grey line shows the one of events generated in the muon Veto itself. The black line is the sum of the two contributions.

REFERENCES

[1] Steigman G. and Turner M. S., *Nucl. Phys. B*, **253** (1985) 375.
[2] Aprile E. *et al.*, *Phys. Rev. Lett.*, **97** (2006) 081302.
[3] Lang Rafael F., McCabe C., Reichard S., Selvi M. and Tamborra I., *Phys. Rev. D*, **94** (2016) 103009.
[4] Aprile E. *et al.*, *Eur. Phys. J. C*, **77** (2017) 881.
[5] The Supernova neutrino data are available from `https://wwwmpa.mpa-garching.mpg.de/ccsnarchive/index.html`.
[6] Pontecorvo B., *Sov. Phys.*, **26** (1968) 984.
[7] Kobayashi M. and Maskawa T., *Prog. Theor. Phys.*, **49** (1973) 652.
[8] Mirizzi A., Tamborra I., Janka H. T., Saviano N., Scholberg K., Bollig R., Hudepohl L. and Chakraborty S., *Riv. Nuovo Cimento*, **39** (2016) 1.
[9] Smirnov A. Yu., *Phys. Scr.*, **T121** (2005) 57.
[10] Agafonova N. Yu. *et al.*, *Astropart. Phys.*, **27** (2007) 254.